nature geoscience

SUPPLEMENTARY INFORMATION

DOI: 10.1038/NGEO2387

Presence of oxygen and aerobic communities from sea floor to basement in deep-sea sediments

Steven D'Hondt[1]*, Fumio Inagaki[1], Carlos Alvarez Zarikian[1], Lewis J. Abrams[2], Nathalie Dubois[1], Tim Engelhardt[1], Helen Evans[1], Timothy Ferdelman[1], Britta Gribsholt[1], Robert N. Harris[1], Bryce W. Hoppie[1], Jung-Ho Hyun[1], Jens Kallmeyer[1], Jinwook Kim[1], Jill E. Lynch[1], Claire C. McKinley[3], Satoshi Mitsunobu[1], Yuki Morono[1], Richard W. Murray[1], Robert Pockalny[4], Justine Sauvage[4], Takaya Shimono[1], Fumito Shiraishi[1], David C. Smith[1], Christopher E. Smith-Duque[1], Arthur J. Spivack[1], Bjorn Olav Steinsbu[1], Yohey Suzuki[1], Michal Szpak[1], Laurent Toffin[1], Goichiro Uramoto[1], Yasuhiko T. Yamaguchi[1], Guo-liang Zhang[1], Xiao-Hua Zhang[1], Wiebke Ziebis[1]

[1] Integrated Ocean Drilling Program Expedition 329 Shipboard Scientific Party.

[2] Center for Marine Science, University of North Carolina at Wilmington, 5600 Marvin K. Moss Lane, Wilmington, NC 28409, USA.

[3] Department of Oceanography, Texas A&M University, College Station, Texas 77843, USA.

[4] Graduate School of Oceanography, University of Rhode Island, Narragansett, RI 02882, USA.

* To whom correspondence should be addressed at University of Rhode Island Graduate School of Oceanography, South Ferry Road, Narragansett, RI 02882, USA. E-mail: dhondt@uri.edu

Supplementary Information

Chemical, physical and geological data

All Expedition 329 chemical, physical and geological data and their measurement protocols are described in reference 1. We present site details and summary results in Table 1. All samples were taken by piston coring in advance of the drill bit[1].

Cell enumeration procedures

We provide the cell-count data for this manuscript in Table 2. These are not the shipboard data in reference 1; the minimum quantification limit (MQL) for the shipboard cell counts (~10^3 cells/cm^3)[1] was too high to conclusively test the presence or absence of microbial cells in the deepest, oldest sediment of our sites. Consequently, we greatly refined the cell-counting protocols and undertook new counts for this manuscript after the expedition.

For cell enumeration, we routinely took 2-cm^3 samples from the center of cut core ends using a 3-cm^3 syringe. Each 2-cm^3 sediment plug was extruded into a sterile 15-ml centrifuge tube containing 8 ml of 2.5% (w/v) NaCl solution with 2 % (v/v) formalin as a fixative, and then thoroughly shaken to form a homogenous suspension. We performed cell counts by a fluorescence color-based cell enumeration technique using SYBR Green I fluorescent dye[2]. To evaluate low-density populations (below 10^4 cells cm^{-3}), we detached cells from sediment by using a multi-layer density gradient technique[3]. For

22 blank samples, we replaced the sediment slurry with sterile-filtered TE Buffer. We then
23 counted cell numbers by either manual or computer-based microscopic observations[2,4].
24 We defined the MQL as the mean of the blank counts plus three times their standard
25 deviation. As shown in manuscript Fig 2, the MQL for these counts is 130 cells/cm^3. We
26 carried out all filter preparation steps, including sonication of sediment and SYBR Green
27 I staining, in an ultra-clean bench placed in a HEPA-filtered clean booth at the Kochi
28 Institute for Core Sample Research, JAMSTEC.
29 We confirmed the presence of dissolved O_2 throughout the sediment column at all six
30 SPG sites by independently undertaking parallel O_2 measurements for each site using
31 fiber-optic O_2 microsensors (optodes)[5] and amperometric Clark-type O_2 sensors
32 (microelectrodes)[6]. For consistency, we used optode data for all O_2 calculations and
33 illustration, except for Sites U1368 and U1371, where optode data are limited to small
34 fractions of the sediment column; at those sites, electrode-based measurements are used
35 for illustration.
36
37 **Calculation of O_2 exposure times**
38 We calculated O_2 exposure times[7] by dividing O_2 penetration depth by sediment age
39 at the depth of O_2 penetration. For Sites U1365 to U1370, O_2 penetration depth equals
40 total sediment thickness and sediment age at the depth of O_2 penetration equals basement
41 age[1]. For Site U1371, we used mean sediment accumulation rate calculated from
42 sediment thickness and basement age to estimate sediment age at depth of O_2 penetration.
43
44 **Comparison of dissolved O_2 to dissolved NO_3^-**

Because O_2 measurements and NO_3^- measurements were made at different sediment depths and (often) in different holes, we interpolated O_2 concentrations for comparison to NO_3^- in SI Fig 1. Because the diffusion coefficient of dissolved O_2 is about 10% higher than that of NO_3^- at *in situ* temperatures[8], O_2 diffuses into the sediment slightly faster than NO_3^- diffuses out. This difference is consistent with the slight excess of NO_3^- relative to the Redfield O_2/NO_3^- respiration ratio in at the sites with greatest sediment thickness (U1365 and U1370). To account for the slight difference in diffusion coefficients of O_2 and NO_3^-, the relationship of O_2 and NO_3^- profiles to the Redfield ratio in subseafloor SPG sediment has been quantitatively tested by use of a diffusion-reaction model for the O_2 and NO_3^- data of Site U1370[9]; this test demonstrated that the best-fit $NO_3^-/-O_2$ respiration ratio is indistinguishable from the Redfield ratio throughout the sediment column.

Reaction rate calculations

We quantified vertical distributions of O_2 reaction (aerobic respiration) rates (Table 3) using the MatLab program and numerical procedures of reference 10, with dissolved O_2 concentrations, physical properties (*in situ* temperature, porosity, formation factor) and sediment burial rates from reference 1. For our calculations, we assumed fluid advection rates to be below detection. We derived our diffusion coefficients from *in situ* temperature data[1] and diffusion coefficients of O_2 in seawater at standard temperatures[8].

The algorithm for calculating reaction rates uses iterative numerical procedures to identify the maximum number of depth intervals with statistically different reaction rates at a prescribed significance level ($\alpha = 0.05$). It explicitly accounts for downhole variation

68 in physical properties and measurement spacing.

69 A key variable in this approach is the user-defined minimum number of data points
70 required to define a reaction zone. We used a minimum of either 5 data points (for Sites
71 U1365, U1367, U1369, U1370)) or 7 data points (for Site U1366) to define the minimum
72 reaction zones for our calculations after testing a range of values from 3-21 data points.
73 Our selection of these minimum reaction zones was based on the fit of an algorithm-
74 derived best-fit line to the actual O_2 measurements and the complexity or variability of
75 the defined reaction rate zones. For example, reaction zones defined by fewer than 5
76 points exhibited nice fits to the actual O_2 data, but the resulting reactions rates were very
77 erratic and unrealistic as the values often alternated rapidly between positive and negative
78 values. This erratic character resulted from rapid changes in slope of the best-fit line used
79 to derive reaction rates. For reaction zones defined by more than 7 points, the best-fit line
80 departed significantly from the actual O_2 measurements, and the reaction zones are
81 typically too broad and underestimated the characteristic reaction rate. Our selection of
82 the 5- or 7-point minimum reaction zone iteration depended on which number of points
83 per minimum zone yielded a lower uncertainty.

84 We used a Monte Carlo technique to estimate uncertainties in the calculated reaction
85 rates[10]. The key variables for the uncertainty estimate are the precision of the O_2
86 measurement and the number of reaction rate iterations. For our results, we used a 1%
87 measurement precision with 50 iterations.

88 At Sites U1365, U1369 and U1370, the program calculated brief intervals of net O_2
89 production for the second reaction zone below the seafloor. These results are essentially
90 indistinguishable from zero (see Table 3 and manuscript Fig 3) and disappear if we

calculate the mean rates over longer data intervals. Their cause is unclear, but their consistent occurrence in the second reaction interval at each site suggests that they may be an artifact of the rapid change in O_2 gradient at this depth and the very small number of data points in this reaction subzone (five).

We calculated per-cell respiration rates from these reaction rates and the cell counts in manuscript Fig 2a. These rates were converted to electron transport rates assuming transfer of 4 electrons per O_2 molecule reduced. We calculated per-cell respiration rates for equatorial Pacific ODP Site 1226 using sulfate reduction rates from reference 10, cell counts from reference 11, and assuming transfer of 8 electrons via reduction of each sulfate ion.

Predicting the global distribution of O_2 and aerobic communities from seafloor to basement

To map where oxygen may be present in the sediment from seafloor to basement, we examined the relationship between O_2 penetration to basement and several relevant variables for which there are globally extrapolated maps; these variables included estimates of mean annual seasurface chlorophyll content[12], particulate organic carbon flux at 2 km waterdepth[13], seafloor carbon deposition flux[14], organic carbon burial rate[15, 16], seafloor oxygen flux[15, 16], oxygen-equivalent carbon flux[16], sediment thickness[17, 18], and mean sedimentation rate (calculated as described below). Global extrapolations of seafloor carbon deposition flux, seafloor oxygen flux and sedimentation rate are generally correlated because seafloor carbon deposition flux and seafloor oxygen flux are typically calculated from estimates of sedimentation rate[e.g., 15, 16].

114 Of these variables, we found the combination of mean sediment accumulation rates
115 and sediment thickness best explained the distribution of sites where dissolved O_2 does or
116 does not penetrate from seafloor to basement. Consequently, we used sediment thickness
117 and mean sediment accumulation rates to create a map that predicts where oxygen is
118 likely to be present throughout the entire sediment column. We created the global
119 sediment accumulation rate map by merging sediment thickness grids[17, 18] and dividing
120 by the basement age grid[19]. For these maps, we resampled the original grids[17-19] at a 5-
121 minute grid interval. We used Generic Mapping Tools software[20] for grid manipulations
122 and calculations.
123 To define combinations of sediment thickness and sediment accumulation rate for
124 regions with oxic sediment to basement, we used dissolved O_2 measurements[1, 21-23] or
125 measurements of dissolved NO_3^- concentrations that approximate or exceed local bottom-
126 water values[24]. At sites where dissolved O_2 measurements approach zero[23], we detrended
127 the data, discarded measurements that lie outside the second standard deviation of the
128 data profile and then determined if zero fell within the second standard deviation of the
129 remaining measurements. To define combinations of sediment thickness and sediment
130 accumulation rate for regions with anoxic sediment at depth, we used profiles of
131 dissolved O_2, NO_3^-, dissolved manganese, dissolved iron, dissolved SO_4^{2-} and dissolved
132 CH_4 from Deep Sea Drilling Project, Ocean Drilling Program and Integrated Ocean
133 Drilling Program sites[25] and profiles of dissolved O_2 from deep piston coring sites[21, 22].
134 We examined dissolved chemical profiles from 401 open-ocean DSDP, ODP and IODP
135 drill sites and 24 long-coring sites that geographically bound the regions of possible O_2
136 penetration to basement (425 total sites). To prevent our results from being affected by

small numbers of bad measurements at individual sites, we limited this analysis to the 149 sites (of the 425) that exhibit smoothly varying concentration profiles for measurements of one or more of these dissolved chemicals. At eight sites, we used dissolved manganese as evidence of O_2 absence, following the standard assumptions that (i) manganese is not reduced in oxic environments[26, 8] and (ii) dissolved manganese is predominantly reduced [Mn(II) and $MnCl^+$ [27] or ligand-stabilized Mn(III)[28]]. However, recent studies have recorded dissolved manganese concentrations of a few micromolar in subseafloor sediment with abundant dissolved O_2 in the South Pacific Gyre[1] and the North Pacific Gyre (R.W. Murray, pers. comm. 8/14); whether these concentrations are sampling artifacts or (meta)stable concentrations of dissolved manganese in strongly oxic sediment remains to be determined.

Assessment of influence on subducting sediment

To assess effects of O_2 penetration depth on the chemistry of subducting sediment, we examined published records of sediment composition at DSDP/ODP/IODP sites seaward of subduction zones. In some regions, sediment sequences that we infer to be fully penetrated by O_2 directly enter a subduction zone (e.g., the Tonga Trench and the central and southern portions of the Peru-Chile Trench) (see manuscript Fig 4). In other regions, sedimentation rate and sediment thickness increase as the trench is approached. Despite anoxia in the upper sediment column of the latter regions, a great deal of oxidized material is present deeper in the sediment. For example, porewater chemical profiles indicate that manganese reduction is dominant in the upper sedimentary column of DSDP Site Sites 1149 and 1231, which respectively approach the Izu-Bonin Trench and the

northern Peru-Chile Trench[29, 11]. In such sequences, dissolved O_2 is not present in the upper sediment column at the time of subduction, but oxidized iron and oxidized manganese may remain abundant in solid phases at greater depth (e.g., DSDP Sites 303, 426, 578 and 581)[30-32] and dissolved O_2 and NO_3^- may be present in the deepest sediment and the upper basement[11].

References

1 D'Hondt, S., Inagaki, F., Alvarez Zarikian, C.A., & the Expedition 329 Scientists, *Proc. IODP* **329**: Tokyo (Integrated Ocean Drilling Program Management International, Inc.) (2011).

2 Morono, Y., Terada, T., Masui, N. & Inagaki, F. Discriminative detection and enumeration of microbial life in marine subsurface sediments. *ISME Journal* **3**, 503-511 (2009).

3. Morono, Y., T. Terada, J. Kallmeyer and F. Inagaki, An improved cell separation technique for marine subsurface sediments: applications for high-throughput analysis using flow cytometry and cell sorting, *Environ. Microbiol*. **15,** 2841-2849 (2013).

4 Morono, Y. & Inagaki, F. Automatic Slide-Loarder Fluorescence Microscope for Discriminative Enumeration of Subseafloor Life. *Scientific Drilling* **9**, 32-36 (2010).

5 Fischer, J. P., Ferdelman, T.G., D'Hondt, S., Røy, H. & Wenzhöfer, F. Oxygen penetration deep into the sediment of the South Pacific gyre. *Biogeosciences* **6**, 1467-1478 (2009).

183 [6] Revsbech, N.P. An oxygen microsensor with a guard cathode. *Limnol. Oceanogr*.
184 **34**, 474-478 (1989).
185 [7] Hartnett, H.E., R.G. Keil, J.I. Hedges and A.H. Devol, Influence of oxygen
186 exposure time on the preservation of organic carbon in continental margin
187 sediments, *Nature* **391** 572-574 (1998).
188 [8] Schulz, H.D. in *Marine Geochemistry*, H. D. Schulz, M. Zabel, Eds. (Springer-
189 Verlag, Heidelberg, New York, 2000), 85–128.
190 [9] Huang, Y., "The NO_3^-/-O_2 respiration ratio of the deep sedimentary biosphere in
191 the Pacific gyres" (2014). *Dissertations and Master's Theses (Campus Access)*.
192 Paper AAI1555654. http://digitalcommons.uri.edu/dissertations/AAI1555654.
193 [10] Wang, G., A.J. Spivack, S. Rutherford, U. Manor and S. D'Hondt, Quantification
194 of co-occurring reaction rates in deep subseafloor sediments, *Geochim.*
195 *Cosmochim. Ac.* 72, 3479-3488 (2008).
196 [11] D'Hondt, S., and 34 others, Distributions of microbial activities in deep
197 subseafloor sediments, *Science* 306, 2216-2221.
198 [12] Global SeaWiFS Chlorophyll (mean of September 1997 - December 2004
199 [13] Henson, S.A., R. Sanders and E Madsen, Global patterns in efficiency of
200 particulate organic carbon export and transfer to the deep ocean, Global
201 Biogeochemical Cycles 26, GB1028 (2012).
202 [14] Dunne, J. P., J.L. Sarmiento, and A. Gnanadesikan, A synthesis of global particle
203 export from the surface ocean and cycling through the ocean interior and on the
204 seafloor, *Global Biogeochem. Cycles* **20** (2007).

205 [15] Jahnke, R.A. and G.A. Jackson, The spatial distribution of sea floor oxygen
206 consumption in the Atlantic and Pacific Oceans, in Rowe, G.T., and Parient, V.,
207 eds., Deep-Sea Food Chains and the Global Carbon Cycle, p. 295-307 (1992).
208 [16] Jahnke, R. A. The global ocean flux of particulate organic carbon: areal
209 distribution and magnitude. *Global Biogeochem. Cycles* **10**, 71-88 (1996).
210 [17] Divins D.L. NGDC Total Sediment Thickness of the World's Oceans & Marginal
211 Seas (NOAA) (2008).
212 [18] Laske, G. and G.A. Masters, global digital map of sediment thickness. *EOS*
213 *Trans. AGU* 78, F483 (1997).
214 [19] Müller R. D., Sdrolias M., Gaina C., & Roest W. R. Age, spreading rates, and
215 spreading asymmetry of the world's ocean crust. *Geochem. Geophys. Geosy.* **9**
216 (2008).
217 [20] Wessel P. & Smith W.H.F. New, inproved version of the Generic Mapping Tools
218 released. *EOS Trans. AGU.* 79, 579 (1998).
219 [21] D'Hondt, S. *et al.* Subseafloor sedimentary life in the South Pacific Gyre. *Proc.*
220 *Nat. Acad. Sci. U.S.A.* **106**, 11651-11656 (2009).
221 [22] Røy, H., J. Kallmeyer, R.R. Adhikari, R. Pockalny, B.B Jørgensen and S.
222 D'Hondt, Aerobic microbial respiration in 86-million-year-old deep-sea red clay,
223 *Science* 336 (6083), 922-925 (2012). Erratum (figure correction) in *Science* 336
224 (6088), 1506 (2012).
225 [23] Orcutt, B.N., et al., Oxygen consumption rates in subseafloor basaltic crust
226 derived from a reaction transport model, *Nat. Commum.* **4**, 2539 (2013).

[24] Gieskes, J.M. and J. Boulegue, Interstitial Water Studies, Leg-92, *Init. Rep. DSDP* **92**, 423-429 (1986).

[25] DSDP/ODP/IODP Core database. College Station, TX: International Ocean Discovery Program. <http://iodp.tamu.edu/database/index.html>

[26] Froelich, P. N., Klinkhammer, G. P., Bender, M. L., Luedtke, N. A., Heath, G. R., Cullen, D., Dauphin, P., Hammond, D., Hartman, B., & Maynard. V. Early oxidation of organic matter in pelagic sediments of the eastern equatorial Atlantic: suboxic diagenesis, *Geochim. Cosmochim. Ac.* **43**, 1075-1090 (1979).

[27] Bruland, K. Trace elements in seawater, in *Chemical Oceanography*, 2nd Edition, Vol. **8** (ed. Riley, J. P., & Chester, R.), Academic, London, 147-220 (1983).

[28] Madison, A. S., Tebo, B. M., Mucci, A., Sundby, B. & Luther, G. W. III, Abundant porewater Mn(III) is a major component of the sedimentary redox system, *Science* **341**, 875-878 (2013).

[29] Shipboard Scientific Party, 2000. Site 1149. *In* Plank, T., Ludden, J.N., Escutia, C., et al., *Proc. ODP, Init. Repts.,* 185 [Online]. Available from World Wide Web: <http://www-odp.tamu.edu/publications/185_IR/chap_03/chap_03.htm>.

[30] Larson, R.L., and 9 others, Site 303: Japanese Magnetic Lineations, in R.L. Larson, R. Moberly et al., *Initial Reports DSDP* **32**, Washington D.C. (U.S. Government Printing Office) (1975).

[31] Shipboard Scientific Party, with P.S. Doyle, 5. Site 578, in G.R. Heath, L.H. Burckle et al., Initial Reports DSDP 86, Washington D.C. (U.S. Government Printing Office) (1985).

[32] Heath, G.R., R.B. Kovar and C. Lopez, Geochemistry of Sediments at Sites 579, 580, and 581, Deep Sea Drilling Project Leg 86, Western North Pacific, in G.R. Heath, L.H. Burckle et al., Initial Reports DSDP 86, Washington D.C. (U.S. Government Printing Office) (1985).

[33] Anderson, L.A. and J.L. Sarmiento, Global ocean phosphate and oxygen simulations. *Glob. Biogeochem. Cy.* **9**, 621-636 (1995).

Table 1. Site properties[1] and depth-integrated O_2 reduction rates below 1.5 mbsf. n.d. = not determinable (no optode data). n.a. = not applicable (O_2 does not penetrate to 1.5 mbsf at U1371).

Site	Latitude	Longitude	Water depth (m)	Seasurface chl-a concentration (mg Chl-a/m^3)	Total sediment thickness (m)	O_2 exposure time (Ma)	O_2 consumption in sediment >1.5 mbsf (mol/cm^2/yr)
Within gyre							
U1365	-23°51'	-165°39’	5695	0.057	75	84 - 120	-2.20E-08
U1366	-26°03'	-156°54’	5127	0.054	30	84 - 120	-6.28E-09
U1367	-26°29'	-137°56’	4289	0.035	27	33.5	-2.03E-09
U1368	-27°55'	-123°10’	3740	0.030	16	13.5	n.d.
U1369	-39°19'	-139°48’	5277	0.110	16	58	-3.24E-09
U1370	-41°51'	-153°06’	5075	0.138	68	75	-1.77E-08
Outside gyre							
U1371	-45°58'	-163°11’	5305	0.199	131	0.035	n.a.

263 **Table 2.** Post-expedition cell counts for Expedition 329 sites. The cell counts shown in
264 manuscript Fig 2a and used for our per-cell reaction rate calculations (Table 3)
265 were limited to counts from sedimentary intervals described by shipboard
266 scientists as characterized by no visible sediment disturbance or only slight
267 disturbance[1]. Counts from sediment described by shipboard scientists[1] as heavily
268 disturbed, moderately disturbed or affected by flow-in were excluded from
269 manuscript Fig 2a and our per-cell calculations. Define disturbance notes of
270 fourth column. The extent of sediment disturbance at each sampling depth is
271 identified in the Disturbance intensity column as follows: H (heavily disturbed),
272 M (moderately disturbed, S (slightly disturbed), F (flow-in). Intervals free of
273 visible disturbance are left blank in the Disturbance intensity column.
274

Site	Hole	core	section	cm interval	Depth (mbsf)	Cell abundance (cells / cm^3)	Disturbance intensity
U1365	B	1	1	40-50	0.5	5.14×10^5	H
U1365	B	1	2	40-50	2.0	5.29×10^4	M
U1365	B	1	3	40-50	3.5	3.02×10^4	M
U1365	B	2	1	75-85	4.9	1.69×10^4	
U1365	B	2	2	140-150	7.1	2.27×10^4	
U1365	B	2	3	75-85	7.9	2.19×10^4	
U1365	B	2	4	75-85	9.4	1.44×10^4	
U1365	B	2	5	75-85	10.9	1.00×10^4	
U1365	B	2	6	75-85	12.4	1.06×10^4	
U1365	B	2	7	58-68	13.7	8.41×10^3	
U1365	B	3	1	75-85	14.4	1.31×10^4	S
U1365	B	3	2	75-85	15.9	1.18×10^4	
U1365	B	3	3	75-85	17.4	8.00×10^3	
U1365	B	3	4	75-85	18.9	1.17×10^4	
U1365	B	3	5	75-85	20.4	1.33×10^4	
U1365	B	3	6	75-85	21.9	4.43×10^3	
U1365	B	3	7	40-50	23.1	5.22×10^3	

U1365	B	4	1	75-85	23.9	6.91×10^{2}	
U1365	B	4	2	75-85	25.4	1.71×10^{3}	
U1365	B	4	3	75-85	26.9	1.69×10^{3}	
U1365	B	4	4	75-85	28.4	4.96×10^{2}	
U1365	B	4	5	75-85	29.9	2.04×10^{3}	
U1365	B	4	6	75-85	31.4	4.96×10^{2}	
U1365	B	4	7	25-30	32.4	3.34×10^{2}	
U1365	B	5	1	75-85	33.4	2.26×10^{2}	
U1365	B	5	2	75-85	34.9	3.08×10^{3}	
U1365	B	5	3	75-85	36.4	1.03×10^{3}	
U1365	B	5	4	75-85	37.9	6.84×10^{2}	
U1365	B	5	5	65-75	39.3	1.43×10^{3}	S
U1365	B	5	6	75-85	40.9	6.64×10^{2}	H
U1365	B	5	7	63-73	42.3	6.67×10^{2}	H
U1365	B	8	2	40-50	65.5	1.33×10^{4}	
U1365	B	8	3	55-65	66.6	8.70×10^{1}	
U1365	B	9	1	140-149	68.4	5.17×10^{3}	
U1365	B	9	2	40-50	69.0	1.01×10^{4}	
U1365	B	9	3	40-50	70.5	3.86×10^{2}	
U1365	B	9	4	40-50	72.0	2.76×10^{3}	
U1365	B	9	5	40-50	73.5	3.60×10^{3}	
U1365	B	9	6	50-60	74.7	4.99×10^{3}	
U1365	B	9	6	50-60	75.1	2.10×10^{3}	
U1365	B	9	6	50-60	75.6	4.55×10^{3}	

U1366	D	1	2	40-50	2.0	2.27×10^{4}	
U1366	D	1	3	40-50	3.5	1.05×10^{4}	
U1366	D	1	4	50-60	5.1	5.23×10^{4}	
U1366	D	1	5	40-50	6.5	5.10×10^{4}	
U1366	D	1	6	40-50	8.0	1.43×10^{5}	
U1366	D	1	7	20-30	9.0	1.71×10^{4}	
U1366	D	2	1	40-50	9.9	3.36×10^{4}	
U1366	D	2	2	40-50	11.4	8.32×10^{3}	
U1366	D	2	3	40-50	12.9	1.11×10^{4}	
U1366	D	2	4	40-50	14.4	5.56×10^{2}	
U1366	D	2	6	40-50	17.2	2.75×10^{3}	
U1366	F	2	2	60-70	7.7	9.15×10^{2}	
U1366	F	2	4	60-70	10.7	1.44×10^{4}	
U1366	F	3	1	40-50	14.5	5.44×10^{3}	H
U1366	F	3	2	40-50	16.0	6.67×10^{3}	
U1366	F	3	3	40-50	17.5	4.99×10^{3}	
U1366	F	3	4	40-50	19.0	8.74×10^{3}	
U1366	F	3	5	40-50	20.5	5.75×10^{3}	
U1366	F	3	6	40-50	22.0	3.55×10^{3}	
U1366	F	3	7	30-41	23.4	2.48×10^{2}	

U1366	F	4	1	40-50	24.0	5.61×10^{3}	H
U1366	F	4	2	40-50	25.3	5.67×10^{3}	
U1366	F	4	2	40-50	25.5	9.81×10^{3}	
U1366	F	4	3	40-50	27.0	5.49×10^{3}	
U1366	F	4	4	0-10	28.1	7.18×10^{3}	
U1366	F	4	5	50-59	29.5	8.84×10^{3}	H
U1366	F	4	5	40-50	30.1	7.47×10^{5}	H
U1367	C	1	1	10-20	0.2	2.31×10^{5}	S
U1367	C	1	2	60-70	2.2	1.91×10^{5}	
U1367	C	1	3	60-70	3.7	3.84×10^{4}	
U1367	C	1	4	60-70	5.2	9.56×10^{5}	
U1367	C	1	5	60-70	6.7	1.06×10^{3}	S
U1367	C	2	1	60-70	7.9	2.82×10^{3}	
U1367	C	2	2	60-70	9.4	1.89×10^{3}	
U1367	C	2	3	60-70	10.9	5.90×10^{3}	
U1367	C	2	4	60-70	12.4	1.70×10^{3}	
U1367	C	2	5	60-70	13.9	1.43×10^{3}	
U1367	C	2	6	60-70	15.4	4.90×10^{3}	
U1367	C	2	7	50-60	16.8	4.79×10^{3}	
U1367	C	3	1	50-60	17.3	1.82×10^{4}	
U1367	C	3	2	0-5	18.2	5.00×10^{3}	
U1367	C	3	3	60-70	20.4	4.38×10^{3}	
U1367	C	3	4	60-70	21.9	2.23×10^{3}	
U1367	C	3	6	0-5	23.6	6.04×10^{3}	F
U1367	D	2	4	50-60	12.5	4.31×10^{5}	S
U1367	D	3	1	80-90	17.8	2.42×10^{4}	S
U1367	D	3	2	10-20	18.6	1.28×10^{6}	S
U1367	D	3	3	10-20	20.1	7.45×10^{4}	S
U1367	D	3	4	80-90	22.3	2.23×10^{3}	S
U1367	D	3	5	80-90	23.8	3.34×10^{2}	
U1367	D	3	6	10-20	24.6	2.85×10^{3}	
U1368	C	1	1	10-15	0.1	1.13×10^{6}	
U1368	C	1	2	60-70	2.2	4.04×10^{6}	
U1368	C	1	3	60-70	3.7	5.45×10^{6}	
U1368	C	1	4	60-70	5.2	1.05×10^{5}	
U1368	C	1	5	40-50	6.5	1.85×10^{5}	
U1368	C	1	6	10-20	7.7	1.04×10^{5}	
U1368	C	2	1	50-60	8.6	3.43×10^{3}	S
U1368	C	2	2	60-70	10.2	5.07×10^{3}	S
U1368	C	2	3	60-70	11.7	2.40×10^{3}	S
U1368	C	2	4	60-70	13.2	7.85×10^{3}	S
U1368	C	2	5	60-70	14.7	2.19×10^{3}	

U1368	C	2	6	10-20	15.6	1.31×10^{5}	H
U1369	C	1	1	15-20	0.2	4.83×10^{5}	H
U1369	C	1	2	50-60	2.1	6.18×10^{3}	H
U1369	C	1	3	50-60	3.6	9.93×10^{2}	
U1369	C	1	4	50-60	5.1	2.85×10^{3}	
U1369	C	2	1	50-60	6.6	2.41×10^{3}	
U1369	C	2	2	50-60	8.1	1.71×10^{3}	
U1369	C	2	3	50-60	9.6	2.16×10^{3}	
U1369	C	2	4	50-60	11.1	9.99×10^{2}	
U1369	C	2	5	50-60	12.6	5.34×10^{3}	
U1369	C	2	6	50-60	14.1	1.24×10^{2}	
U1369	C	2	7	45-54	15.5	1.09×10^{4}	
U1369	E	2	6	90-100	15.3	1.38×10^{4}	
U1370	E	1	1	35-42.5	0.4	9.55×10^{5}	S
U1370	E	1	2	30-40	1.9	1.88×10^{5}	
U1370	E	1	3	30-40	3.4	1.07×10^{5}	
U1370	E	1	4	147-152	6.0	8.67×10^{4}	
U1370	E	2	1	135-140	7.6	2.62×10^{3}	
U1370	E	2	2	135-140	9.1	8.31×10^{3}	
U1370	E	2	3	135-140	10.6	2.19×10^{3}	
U1370	E	2	4	125-130	12.0	7.58×10^{3}	
U1370	E	2	5	135-140	13.6	1.81×10^{4}	
U1370	E	2	6	118-123	14.9	4.53×10^{3}	
U1370	E	3	1	135-140	17.1	8.19×10^{3}	
U1370	E	3	2	135-140	18.6	6.78×10^{3}	
U1370	E	3	3	135-140	20.1	2.11×10^{3}	
U1370	E	3	4	125-130	21.5	5.11×10^{3}	
U1370	E	3	5	135-140	23.1	2.12×10^{3}	
U1370	E	3	6	53-58	23.8	2.76×10^{3}	
U1370	E	4	1	135-140	26.6	3.79×10^{3}	
U1370	E	4	2	135-140	28.1	1.43×10^{3}	
U1370	E	4	3	135-140	29.6	1.03×10^{3}	
U1370	E	4	4	125-130	31.0	2.78×10^{3}	
U1370	E	4	5	135-140	32.6	6.91×10^{2}	
U1370	E	5	1	135-140	36.1	8.61×10^{3}	
U1370	E	5	2	129-134	37.5	5.67×10^{3}	
U1370	E	5	3	135-140	39.0	6.05×10^{3}	
U1370	E	5	4	125-130	40.4	7.71×10^{3}	
U1370	E	5	5	135-140	42.0	8.93×10^{3}	
U1370	E	5	6	55-60	42.7	5.97×10^{3}	
U1370	E	6	1	135-140	45.6	2.48×10^{3}	
U1370	E	6	2	124-134	47.0	3.91×10^{3}	

U1370	E	6	3	135-140	48.5	1.85×10^{3}	
U1370	E	6	4	135-140	50.0	1.47×10^{3}	
U1370	E	6	5	95-100	51.1	7.23×10^{3}	
U1370	E	8	2	135-140	58.3	2.06×10^{3}	H
U1370	E	8	3	135-140	59.8	5.08×10^{3}	F
U1370	E	8	4	125-130	61.2	7.13×10^{3}	F
U1370	E	8	5	135-140	62.8	3.74×10^{3}	F
U1370	E	9	1	135-140	63.5	6.57×10^{3}	F
U1370	E	8	6	135-140	64.3	6.57×10^{3}	F
U1370	E	9	2	135-140	65.0	4.43×10^{3}	F
U1370	F	5	3	135-140	39.6	4.87×10^{3}	
U1370	F	5	4	135-140	41.1	4.06×10^{3}	
U1370	F	5	5	135-140	42.6	3.90×10^{3}	
U1370	F	6	2	135-140	47.6	5.50×10^{3}	
U1370	F	6	3	135-140	49.1	5.68×10^{3}	
U1370	F	6	4	135-140	50.6	4.41×10^{3}	
U1370	F	6	5	135-140	52.1	6.17×10^{3}	
U1370	F	7	1	135-140	55.6	3.65×10^{3}	
U1370	F	7	2	135-140	57.1	1.45×10^{3}	
U1370	F	7	3	135-140	58.6	2.29×10^{3}	
U1370	F	7	4	125-130	60.0	3.94×10^{3}	
U1370	F	7	5	135-140	61.6	7.09×10^{3}	
U1370	F	7	6	135-140	63.1	2.19×10^{3}	

U1371	E	1	1	30-40	0.4	4.91×10^{5}	H
U1371	E	1	2	30-40	1.9	2.37×10^{5}	
U1371	E	1	3	30-40	3.4	4.65×10^{5}	
U1371	E	1	4	135-140	5.9	1.29×10^{6}	
U1371	E	1	5	135-140	7.4	1.48×10^{5}	
U1371	E	1	6	52-57	8.0	2.33×10^{5}	
U1371	E	2	1	135-140	9.6	1.25×10^{5}	
U1371	E	2	2	135-140	11.1	9.06×10^{4}	
U1371	E	2	3	135-140	12.6	1.24×10^{5}	
U1371	E	2	4	135-140	14.1	5.41×10^{4}	
U1371	E	2	5	90-95	15.1	1.07×10^{5}	
U1371	E	3	2	135-140	20.6	1.05×10^{5}	
U1371	E	3	3	125-130	22.0	1.38×10^{5}	
U1371	E	3	4	135-140	23.6	1.27×10^{5}	
U1371	E	3	5	115-120	24.9	6.93×10^{4}	
U1371	E	3	6	41-46	25.4	9.82×10^{4}	
U1371	E	4	1	135-140	28.6	3.45×10^{5}	
U1371	E	4	2	135-140	30.1	4.05×10^{3}	
U1371	E	4	3	135-140	31.6	2.85×10^{4}	
U1371	E	4	4	135-140	33.1	2.38×10^{4}	
U1371	E	4	5	115-120	34.4	1.34×10^{4}	

U1371	E	5	1	135-140	38.1	6.20×10^{3}	
U1371	E	5	2	135-140	39.6	2.85×10^{3}	
U1371	E	5	3	135-140	41.1	4.07×10^{3}	
U1371	E	5	4	135-140	42.6	8.15×10^{3}	
U1371	E	5	5	60-65	43.3	1.53×10^{4}	
U1371	E	6	3	135-140	50.6	7.95×10^{3}	H
U1371	E	6	5	135-140	53.6	5.16×10^{3}	
U1371	E	7	1	135-140	57.1	5.11×10^{3}	H
U1371	E	7	2	135-140	58.6	3.61×10^{3}	
U1371	E	7	3	125-130	60.0	5.20×10^{3}	H
U1371	E	7	5	135-140	63.1	2.84×10^{3}	
U1371	E	8	1	135-140	66.6	2.81×10^{3}	H
U1371	E	8	3	135-140	69.6	5.76×10^{3}	
U1371	E	8	5	135-140	72.6	6.91×10^{3}	
U1371	E	9	2	135-140	76.5	1.33×10^{4}	
U1371	E	9	4	135-140	79.5	2.17×10^{3}	
U1371	E	9	6	135-140	82.5	2.25×10^{3}	
U1371	E	10	1	135-140	85.6	2.79×10^{3}	
U1371	E	10	3	135-140	88.6	6.97×10^{3}	
U1371	E	10	5	135-140	91.6	1.13×10^{4}	
U1371	E	11	1	135-140	95.1	2.35×10^{4}	
U1371	E	11	3	125-130	98.0	2.32×10^{3}	
U1371	E	11	5	135-140	101.1	9.46×10^{3}	
U1371	E	12	2	135-140	106.1	6.86×10^{2}	
U1371	E	12	3	125-130	107.5	4.30×10^{3}	
U1371	E	12	4	108-118	108.8	6.66×10^{3}	
U1371	E	13	1	135-140	114.1	3.10×10^{3}	
U1371	E	13	2	135-140	115.6	6.89×10^{3}	
U1371	E	13	3	125-130	117.0	3.02×10^{3}	
U1371	E	13	4	135-140	118.6	7.68×10^{3}	
U1371	E	13	5	135-140	120.1	1.99×10^{3}	
U1371	E	13	6	135-140	121.6	1.43×10^{4}	
U1371	E	13	7	24-29	122.0	5.19×10^{3}	
U1371	E	14	1	135-140	123.6	1.08×10^{4}	
U1371	E	14	2	135-140	125.1	3.79×10^{3}	
U1371	E	14	3	30-40	125.6	4.78×10^{3}	
U1371	E	14	5	30-40	128.6	3.32×10^{2}	
U1371	E	14	6	51-56	130.2	1.57×10^{4}	F

275
276

277 **Table 3.** Vertical distribution of O_2 reaction rates (net respiration) at Expedition 329

278 sites**.**

Interval	# data points in each zone	Depth (mbsf)	Reaction rate ± 1*sigma (mol O_2/cm^3/yr)	Net respiration rate per cell ± 1*sigma (mol O_2/cell/yr)
Site U1365				
1	4	0.25 - 2.18	-8.68E-11 ± 3.68E-11	-3.06E-16 ± 3.76E-16
2	5	2.38 - 4.69	4.63E-12 ± 1.86E-11	1.97E-16 ± 7.95E-16
3	6	4.89 - 8.76	-1.52E-11± 8.49E-12	-6.83E-16 ± 3.82E-16
4	25	8.95 - 12.81	-9.28E-13 ± 6.13E-12	-9.98E-17 ± 6.60E-16
		24.95 - 27.20	-9.28E-13 ± 1.27E-12	-5.46E-16 ± 7.45E-16
		27.95 - 30.95	-9.28E-13 ± 3.84E-12	-7.33E-16 ± 3.10E-16
		31.18 - 37.95	-9.28E-13 ± 1.95E-12	-8.99E-16 ± 2.15E-16
5	13	64.45 - 65.95	-8.45E-12 ± 2.52E-12	-1.26E-15 ± 1.80E-15
		69.04 - 71.05	-8.45E-12 ± 1.96E-12	-1.52E-15 ± 1.13E-15
		74.45 - 75.05	-8.45E-12 ± 1.96E-12	-2.96E-15 ± 1.30E-15
Site U1366				
1	7	0.25 - 2.26	-6.27E-11 ± 2.22E-11	-2.77E-15 ± 1.44E-15
2	22	2.41 - 2.87	-2.67E-12 ± 1.25E-11	-8.49E-17 ± 4.04E-17
		3.03 - 8.27	-2.67E-12 ± 2.36E-12	-3.93E-17 ± 5.29E-17
		8.43 - 11.82	-2.67E-12 ± 2.88E-12	-1.45E-16 ± 1.79E-16
		11.98 - 14.29	-2.67E-12 ± 9.78E-12	-2.75E-16 ± 1.01E-16
		14.45 - 14.76	-2.67E-12 ± 9.84E-12	-8.90E-16 ± 3.44E-16
Site U1367				
1	8	0.05 - 0.5	-5.34E-10 ± 1.70E-10	-2.13E-15 ± 7.89E-16
		0.65 - 1.10	-5.34E-10 ± 1.28E-10	-2.79E-15 ± 1.71E-15
2	19	1.70 - 3.35	-1.55E-12 ± 1.73E-11	-8.11E-18 ± 3.11E-18
		3.50 - 3.80	-1.55E-12 ± 1.65E-11	-3.12E-18 ± 3.34E-18
		3.95 - 5.75	-1.55E-12 ± 5.36E-12	-3.24E-18 ± 1.27E-18
		5.90 - 18.8	-1.55E-12 ± 9.67E-13	-1.04E-17 ± 2.72E-17
Site U1369				
1	6	0.3 - 1.32	-1.72E-10 ± 6.35E-12	-3.56E-16 ± 2.49E-16
2	5	1.44 - 4.98	4.43E-12 ± 6.35E-13	1.33E-15 ± 1.06E-15
3	14	5.10 - 14.00	-3.59E-12 ± 1.51E-13	-1.69E-15 ± 1.42E-15
Site U1370				
1	15	0.05 - 1.64	-3.38E-10 ± 2.45E-12	-5.19E-16 ± 5.61E-16
2	12	1.81 - 6.23	7.64E-13 ± 7.42E-13	7.88E-18 ± 7.74E-18
3	12	6.40 - 15.22	-5.04E-12 ± 5.32E-13	-6.98E-16 ± 5.74E-16
4	13	15.40 - 37.29	-2.39E-12 ± 1.22E-13	-6.08E-16 ± 4.18E-16
5	37	37.46 - 68.00	-3.28E-13 ± 3.92E-14	-6.98E-17 ± 3.14E-17

279

Fig 1. Dissolved O_2 concentrations vs. dissolved NO_3^- concentrations at Sites U1365-U1370. Symbol colors as in manuscript Fig 1. Most data closely match the Redfield ratio [black line[33]]. Data from the two sites with thinnest sediment (youngest) basement (U1367 and U1368) fall below the Redfield line because their O_2 concentrations are primarily controlled by O_2 loss to the underlying basement. Data from below 30 mbsf at U1370 fall below Redfield at low O_2 concentrations because NO_3^- concentrations at greater depth are affected by loss to the underlying basement. These non-Redfield losses (of O_2 to the basement at U1367 and U1368, and of NO_3^- to basement at U1370) are consistent with non-heterotrophic (lithotrophic) microbial processes in the basement.

Fig 2. Regions where we predict dissolved O_2 and aerobic activity to persist from seafloor to igneous basement, based on sediment thickness and mean sediment accumulation rates. (A) Sediment accumulation rate and sediment thickness at sites where O_2 does or does not penetrate to basement. Sediment thicknesses at these sites were determined by direct measurement (drilling or piston-coring to basement). Red dots indicate sites where dissolved O_2 diffusively penetrates the entire sediment column (up to 75 mbsf)[1, 21, 24]. Black dots indicate sites where dissolved O_2 disappears in cm to meters below the seafloor[1, 11, 21-24,]. Yellow dots indicate sites where dissolved O_2 penetrates more than 7 to 34 mbsf and may penetrate to basement but O_2 content is not fully characterized throughout the entire sediment column[21, 22, 24]. (B) Global map predicted from relationships in (A), combined with mean sediment thicknesses and mean sediment accumulation rates defined by standard global maps of sediment thickness[17, 18] and seafloor

303 age[19] averaged over fine-minute grids.

304 The blue areas in 2A and 2B are defined by combinations of sediment
305 thickness and mean sediment accumulation where O_2 is known to penetrate the
306 entire sediment sequence; they represent a minimum estimate of the area over
307 which dissolved O_2 permeates the entire sediment sequence and the upper
308 basement (9% of global seafloor in 2B). The green areas are defined by
309 combinations where O_2 may penetrate the entire column but chemical data
310 resolution is too low to be certain (13% of seafloor in 2B). The orange areas mark
311 combinations of mean sediment accumulation and sediment thickness for which
312 O_2 may penetrate to basement but there are no O_2 or NO_3^- data (3% of seafloor in
313 2B). Because estimated mean sediment thicknesses in five-minute grids
314 throughout the ocean[17, 18] often differ from local sediment thicknesses determined
315 by drilling or piston-coring to basement, not all sites where O_2 penetrates to
316 basement in 2A are located in the blue areas in 2B. The combined yellow, green
317 and blue areas in both 2A and 2B are defined by the combinations of mean
318 sedimentation rates and sediment thicknesses from the standard sediment-
319 thickness maps[17, 18] that include all locations where dissolved O_2 is known to
320 locally penetrate the entire sediment column (34% of seafloor in 2B). The sum of
321 the blue, green, yellow and orange regions represents a maximum estimate of the
322 area over which dissolved O_2 permeates the entire sediment sequence from the
323 seafloor (37% of total seafloor in 2B). These collective regions broadly include all
324 areas of abyssal clay and slowly accumulating carbonate ooze in the world ocean.
325

326 Fig 1.

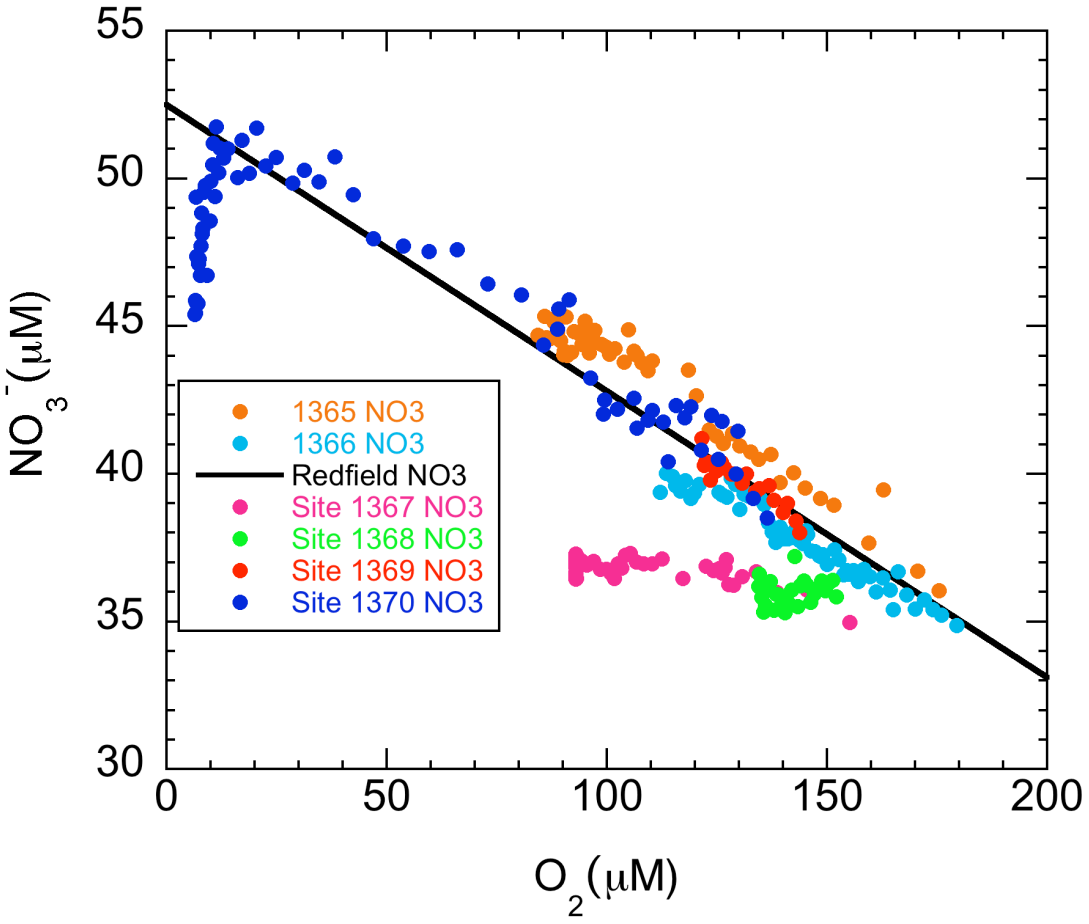

327

328

329 Fig 2A.

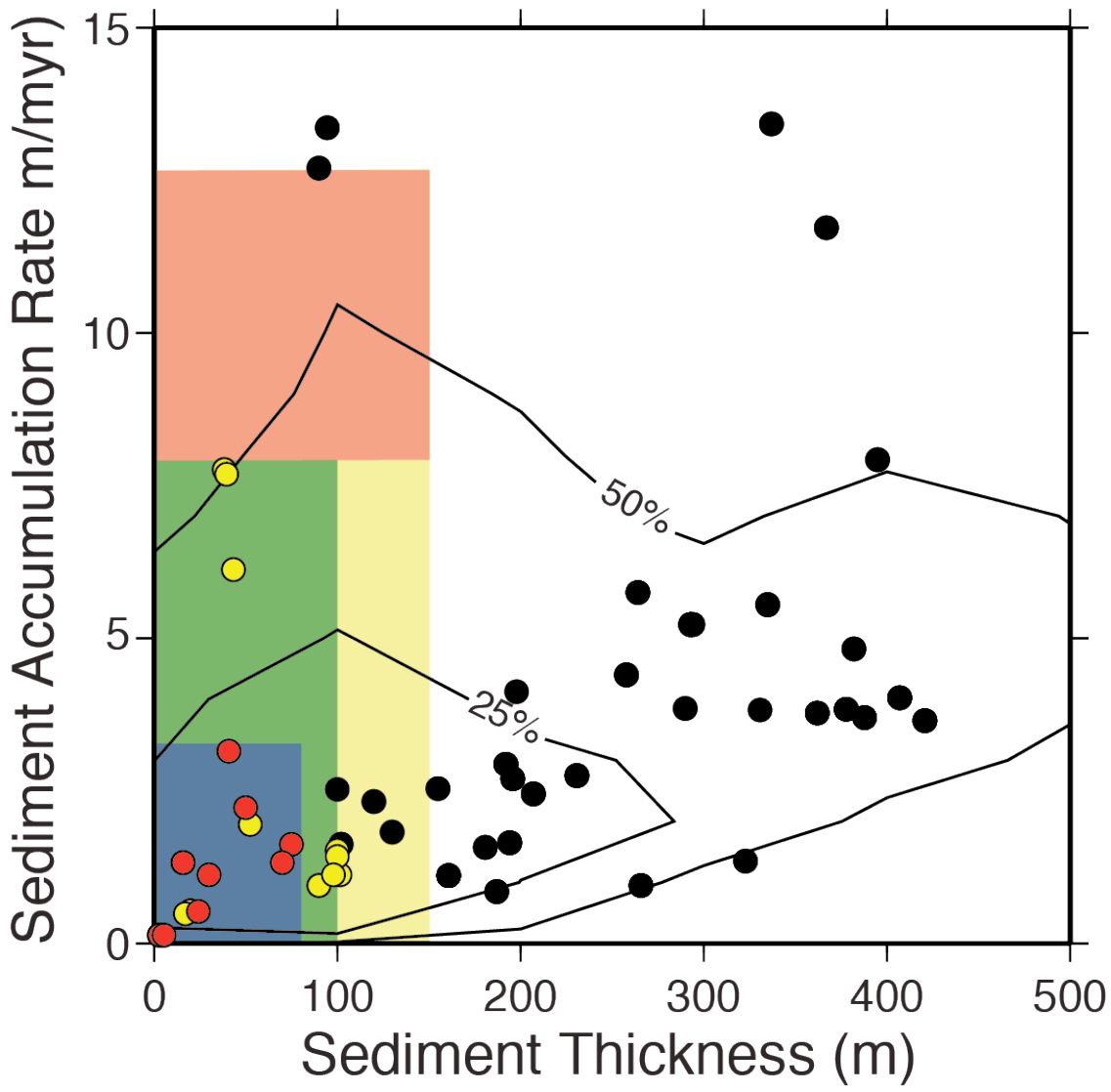

330

331

Fig 2B.